# Three dimensional analysis of histone methylation patterns in normal and tumor cell nuclei

M. Cremer,\*° R. Zinner,\* S. Stein,# H. Albiez,\* B. Wagler,\*° C. Cremer,# T. Cremer\*

*Department of Biology II, Ludwig Maximilians University, Munich; °Institute of Human Genetics, Technical University and GSF; #Kirchhoff Institute of Physics, University of Heidelberg, Germany

Histone modifications represent an important epigenetic mechanism for the organization of higher order chromatin structure and gene regulation. Methylation of position-specific lysine residues in the histone H3 and H4 amino termini has been linked with the formation of constitutive and facultative heterochromatin as well as with specifically repressed single gene loci. Using an antibody, directed against dimethylated lysine 9 of histone H3 and several other lysine methylation sites, we visualized the nuclear distribution pattern of chromatin flagged by these methylated lysines in 3D preserved nuclei of normal and malignant cell types. Optical confocal serial sections were used for a quantitative evaluation. We demonstrate distinct differences of these histone methylation patterns among nuclei of different cell types after exit of the cell cycle. Changes in the pattern formation were also observed during the cell cycle. Our data suggest an important role of methylated histones in the reestablishment of higher order chromatin arrangements during telophase/early G1. Cell type specific histone methylation patterns are possibly causally involved in the formation of cell type specific heterochromatin compartments, composed of (peri)centromeric regions and chromosomal subregions from neighboring chromosome territories, which contain silent genes.

Cell type specific differences of nuclear size, shape and chromatin texture, a parameter for DNA heterogeneity, have been reported for a long time, but the underlying genetic and epigenetic causes of these differences and their functional implications have remained a puzzle. In 1928 the concept of heterochromatin was first described by Heitz (Heitz, 1928), based on his light-microscopic studies of mosses. Heitz named intensely stained nuclear areas *heterochromatin* and less intensely stained areas *euchromatin* and predicted that heterochromatic areas were *genetically passive* and would not contain genes, whereas euchromatin implied *active* or *potentially active* gene-containing regions.

To date, heterochromatin is conventionally classified into two groups: constitutive and facultative heterochromatin. Constitutive heterochromatin is mostly found around (peri)centromeric regions and consists of large (> 1 Mb) arrays of tandemly repeated sequences. Facultative heterochromatin, containing single copy sequences as well as a variety of repetitive sequences, cannot be defined at the level of characteristic DNA sequences, but it reflects an epigenetic state of chromatin. The best-known example is the inactive X in nuclei of female mammals. Euchromatin can be transformed into facultative heterochromatin by epigenetic modifications of DNA and histones. These epigenetic mechanisms include methylation of cytosins at CpG sites, as well as methylation and acetylation at specific sites of histone tails (for review see Bird, 2002) and play an important part in the activation or repression of gene activity. DNA methylation, histone hypoacetylation and histone methylation involved in the formation of facultative heterochromatin are in principle identical to the epigenetic modifications seen in constitutive heterochromatin (for reviews see Bird, 2002; Elgin and Grewal, 2003; Jones and Baylin, 2002; Lachner et al., 2003; Sims et al., 2003).

Nuclei of tumor cells differ in the amount and distribution of heterochromatin from their normal progenitor cells. This fact has widely been used in histopathological diagnosis of tumor cells. Numerous studies of morphometric, densitometric and textural chromatin features were performed with Feulgen stained nuclei to quantitate cell type specific features of chromatin texture and of changes that occur during tumor progression (Diaz et al., 1997; Gil et al., 2002; Mairinger et al., 1999; Mulder et al., 1992; Weyn et al., 2000 b). During the last few years a wealth of information has accumulated for many tumor types on specific mutations, chromosomal translocations, gains and losses of chromosomal subsegments and on gross genomic instabilities. The application of cDNA-array techniques has made it possible to also analyze in detail changes of the expression patterns in tumor cells in comparison to normal cells. In spite of these important advancements, we still know little about the putative functional links between the observed differences of chromatin patterns in normal and malignant cell types and changes of gene expression patterns that occur during tumor progression at the molecular and cytogenetic level.

Antibodies specifically directed against epigenetic markers offer new tools to analyze the spatial arrangement of chromatin on a basis that correlates functional aspects with chromatin topology. Histone tail methylation can be linked to both active chromatin (such as metH3-K4, metH3-K36 and metH3-K79) or repressed chromatin (such as metH3-K9, metH3-K27 and metH4-K20) (for review see Lachner et al., 2003). MetH3-K9 flags specifically repressed gene loci as well as constitutive heterochromatin and creates a binding site for the histone-binding heterochromatin-associated protein 1 (HP1) (Lachner et al., 2001), which is essential for establishing constitutive heterochromatic domains. MetH3-K27 especially marks the inactive X (Plath et al., 2003). The organization of such bulk chromosomal regions can be considered as the *chromosome level* function of histone methylation. Mechanisms by which active genes in euchromatic domains are silenced by lysine methylation mediated processes that have not yet been fully disclosed can be considered as the *gene level* function of histone methylation (for reviews see Elgin and Grewal, 2003; Lachner and Jenuwein, 2002; Lachner et al., 2003; Sims et al., 2003). In this paper we report patterns of (hetero)chromatin marked by methylated lysines at different positions of H3 and H4 in different normal and tumor cells and during defined cell cycle stages. We used an antibody primarily directed against metH3-K9 but it was found that it also broadly reacts with other methylated lysines independent of the respective lysine position (Perez-Burgos et al., 2004), further referred to as multi-methyl lysine (MML) antibody. We demonstrate distinct differences of these patterns among cell types and during cell cycle progression. We present and discuss approaches towards a quantitative 3D evaluation of these patterns.

## Materials and Methods

### Cell material and slide preparation

Human lymphocytes and monocytes from a healthy donor were isolated from peripheral blood by a Ficoll gradient. These cells were either directly mounted on a cover slip before further processing (see below), or cultivated for 60 hours after stimulation with phyto-hemagglutinine in order to obtain cycling lymphocytes. The cell line Jurkat, established from a patient with an acute T cell leukemia (Schneider et al., 1977), has a stable karyotype with an X/18 translocation and a trisomy 20 (Muller et al., 2004). Primary female human diploid fibroblasts were obtained from early passages. Paraffine embedded sections of normal human colon and colon carcinoma tissue were kindly provided by J. Diebold, University of Munich. The breast cancer cell line MCF-7 was provided by P. Meltzer (NIH, Bethesda, MD, USA). M-FISH analysis of the cell passage used for our analysis was kindly performed by A. Jauch, University of Heidelberg and revealed a hypertriploid karyotype (n = 76) with numerous chromosomal rearrangements.

Adherently growing fibroblasts and MCF-7 cells were cultivated on coverslips in the appropriate culture medium until subconfluency. Thirty min before fixation cells were pulse-labeled with BrdU (5 μM final concentration) for the later identification of S phase nuclei. Cells growing in suspension (Jurkat cells, lymphocytes and monocytes) were allowed to attach on polylysine–coated slides for 30 min before fixation. For the preparation of 3D preserved nuclei cells were fixed in 4% paraformaldehyde/PBS and permeabilized in 0.5% Triton X-100/PBS for 5 min. Slides were stored in 1× PBS

at 4°C up to a few days until use. Tissue sections mounted on coverslips were deparaffinized by two successive 30 min incubations in xylole, rehydrated in a descending series of ethanol and rinsed in dd H₂O. Epitope retrieval was performed by microwaving the tissue for 6×5 min at 700 W in 10 mM Na-Citrate pH 6.0. After cooling down to room temperature the sections were transferred to PBS and used for immunostaining.

### Assessment of the cell cycle stage

Detection of BrdU was performed as described by Tashiro et al. (2000). Briefly, after blocking in 5% bovine serum albumine/PBS for 15 min, cells were incubated with mouse-anti-BrdU antibodies (Roche) in 1% BSA, 0.5 × PBS, 30 mM Tris (pH = 7.4), 0.3 mM MgCl₂, 0.5 mM 2-mercaptoethanol and 10 µg/ml DNAse I (Roche). As a secondary antibody goat-anti-mouse Alexa 488 or goat-anti-mouse Alexa 350 (Molecular probes) was applied. A monoclonal antibody against the cell cycle related nuclear protein pKi67 (mouse-anti-pKi67, Dianova) was used for the identification of cells in $G_0$ and early $G_1$ phase and visualized with the same secondary antibody as used for the BrdU detection.

### Visualization of heterochromatin by immunodetection of histone methylation with the MML antibody

An antibody, named multi-methyl lysine (MML), raised in rabbit against 4x branched histone 3 peptide, dimethylated at lysine 9 (K9) position was used. In addition to metH3-K9 this antibody reacts also with tri-methylated H3-K27 and several other methylated lysines independent of their respective positions (Perez-Burgos et al., 2004). Detection was performed by a goat-anti-rabbit antibody conjugated either with Cy3 or Alexa 488 (Molecular probes).

### Visualization of centromeres by immunostaining with a CREST- antiserum

For the delineation of centromeric regions a human antibody directed against centromere specific proteins (Euroimmun) was used and detected with a Cy3- conjugated anti-human antibody.

### DNA counterstain

Nuclear DNA was counterstained with 1 µM TO-PRO-3 (Molecular Probes) for 5 min.

### Confocal microscopy and 3D reconstruction of image stacks

Nuclei were scanned with an axial distance of 250 nm between light optical sections using a three-channel laser scanning confocal microscope (Zeiss LSM 410). For each optical section images were collected sequentially for all three fluorochromes. Stacks of 8-bit gray scale 2D images were obtained with a pixel size of 66 or 88 nm. Confocal images were processed with ImageJ (*http://rsb.info.nih.gov/ij/*).

### Quantitative 3D evaluation

*Threshold assessment*

If not stated otherwise a fixed threshold was set manually for each nucleus after visual inspection in an attempt to segment specific signals from apparent background. All voxels (volume based elements) with intensity values below the threshold were set to 0 and were not counted in the respective evaluations.

*Evaluation of the radial distribution of MML labeled chromatin*

A detailed description of the quantitative 3D evaluation of the radial distribution i.e the distance from the nuclear center to the nuclear periphery of fluorochrome labeled targets in 3D image stacks of light optical serial sections was published elsewhere (Cremer et al., 2003). As a first step the geometrical center and the border of each nucleus were determined using the 3D data set of the DNA-counterstain fluorescence. The segmented nuclear space was divided into 25 equidistant shells with a thickness of $\Delta r = 1/25$ r. In the second step, chromatin delineated after MML immunostaining was evaluated in the 3D stack representing the respective color channel. For each voxel located in the segmented nucleus the relative distance $r_x$ from the nuclear center was calculated as a fraction of r. A shell at a given $r_x$ contains all nuclear voxels with a distance between $r_x - \Delta r/2$ and $r_x + \Delta r/2$. For each shell all voxels assigned to the MML immunostaining were identified and the fluorescence intensities derived from the respective emission spectrum were summed up. This procedure yielded for each shell the individual relative content of MML stained chromatin. This relative content within a nuclear shell was plotted as a function of the relative distance r from the 3D center in the entire set of evaluated nuclei. The cumulative frequencies of voxel intensities plotted against the relative radius were

tested for significant differences ($p \leq 0.01$) with a two-sample Kolmogorov-Smirnov test.

*Definition of objects stained with MML antibodies*

The 8 bit image stack visualizing immunostained metH3-K9 was used for the definition of *objects* in the following ways: An object was defined by the fact that it contained at least ten voxels with a contingent neighborship. Neighborship was defined for all voxels above threshold sharing at least one common side by the software Volocity (*Improvision, http://www.improvision.com/)*, see Figures 5 and 6. For a program written by S. Stein neighborship was defined for all voxels sharing at least one common corner, edge or side (see Figures 4 and 7). The first definition allows for six neighbors/voxel, the second definition for 26 neighbors/voxel. Object counting was done for different threshold settings in intervals of five gray levels until the maximal threshold of 255 was reached. 3D image reconstructions of objects were done with the software Volocity.

*Assessment of the density of MML labeled chromatin*

The average density of MML labeled objects for a given set of nuclei was estimated in two ways: For the first approach the sum of voxel intensities assigned to an object at a given threshold was divided by the sum of the respective voxels (I/vox). For the second approach the sum of voxel intensities assigned to an object at a given threshold was divided by the total surface area of all objects (I/surf). The surface of an object is defined by all voxel sides not attached to other object voxels. This value ($1/\mu m^2$) was taken as a parameter of the compactness of objects. To test for significant differences ($p \leq 0.05$) the Mann-Whitney-U test, a distribution-independent rank test for independent samples was applied.

## Results

### MML stained patterns are distinctly different in different cell types

The characteristic nuclear pattern of chromatin visualized after immunostaining using the MML antibody (further referred to as MML chromatin pattern) and after DNA counterstaining with TO-PRO-3 in different normal and malignant human cell types is shown in Figure 1. The upper row displays the DNA counterstain of a typical confocal mid-section from nuclei of a monocyte (A), a lymphocyte (B), a leukemic T-cell line Jurkat (C), a normal fibroblast (D), a normal colon epithelial cell (E) and a colon adenocarcinoma cell (F). The mid row represents the MML pattern and the bottom row the merged image of the respective nuclei. All nuclei were in a postmitotic state (further referred to as $G_0$), as revealed by their lack of pKi67 staining (Gerdes et al., 1984). These examples illustrate the variability of histone methylation patterns, ranging from a fairly homogeneous pattern with an adumbrated peripheral accumulation in $G_0$ lymphocytes, over a granular pattern seen in fibroblasts, to patterns, which exhibit few large and distinct clusters in monocytes and normal colon epithelial cells. The clusters of intensely stained MML chromatin are not in all cases reflected by a corresponding high staining intensity of the nuclear counterstain (e.g. compare panels A and C). The comparison of MML patterns between representative normal lymphocyte nuclei and nuclei from the T-cell derived leukemic cell line Jurkat revealed distinct differences. In contrast to the commonly observed pattern of a rather homogeneous distribution of MML chromatin in normal $G_0$ lymphocytes, numerous distinct clusters of MML chromatin were observed in nuclei of the Jurkat cell line. A more peripheral accumulation of MML chromatin is seen in the nucleus of the colon carcinoma compared to nuclei of normal colon epithelial cells.

### MML chromatin patterns change during the cell cycle

The MCF-7 cell line was analyzed for changes of the MML chromatin pattern during the cell cycle: We assessed this pattern for nuclei in $G_0$ as defined by a negative staining of pKi67, for nuclei during early $G_1$, identified by a speckled pattern of pKi67 and a faint outlining of the nucleolar space (Gerdes et al., 1984), and for nuclei in early and mid S phase defined by their typical patterns of replication foci visualized by immunostaining of incorporated BrdU. Replication foci of early replicating gene rich chromatin are distributed throughout the nucleus sparing the utmost nuclear periphery and the perinucleolar regions (Figure 2, panel III B), whereas the gene poor mid replicating chromatin forms a typical layer both at the nuclear periphery and around nucleoli (Figure 2, panel III C), (O'Keefe et al., 1992).

Typical examples for each cell cycle stage are depicted in Figure 2. Panel I outlines one confocal
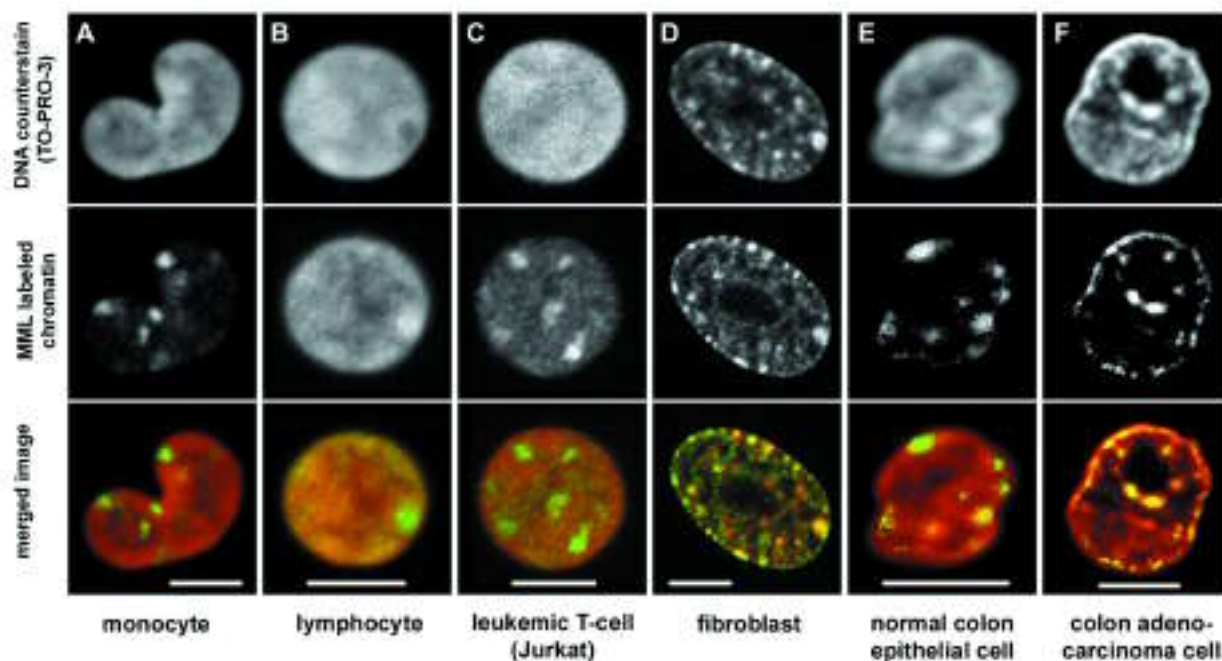
**Figure 1. Chromatin pattern visualized by MML immunostaining in confocal sections from nuclei of different cell types. For each cell type one nucleus is displayed after DNA counterstain with TO-PRO-3 (upper row), the corresponding MML pattern (mid row) and the merged image (bottom row). Bars indicate 5 μm.**
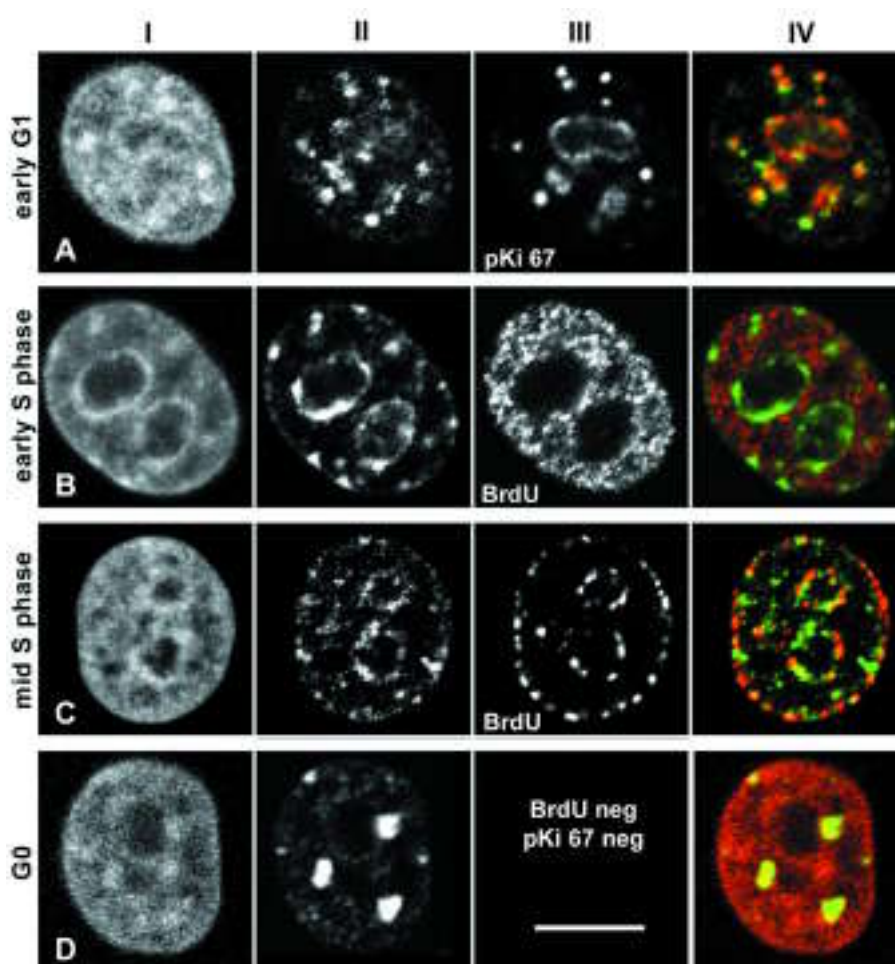


Figure 2. Chromatin pattern visualized by MML immunostaining in nuclei of the MCF-7 cell line during different cell cycle stages. Each panel (A–D) shows a confocal mid-section of a nucleus and represents a different cell cycle stage. Panel I displays the nuclear counterstain by TO-PRO-3, panel II the corresponding MML pattern, panel III either pKi67 or BrdU pattern and panel IV the merged image (MML chromatin in green, pKi67, BrdU or counterstain respectively in red). For a detailed description see results. Bar indicates 5 μm.
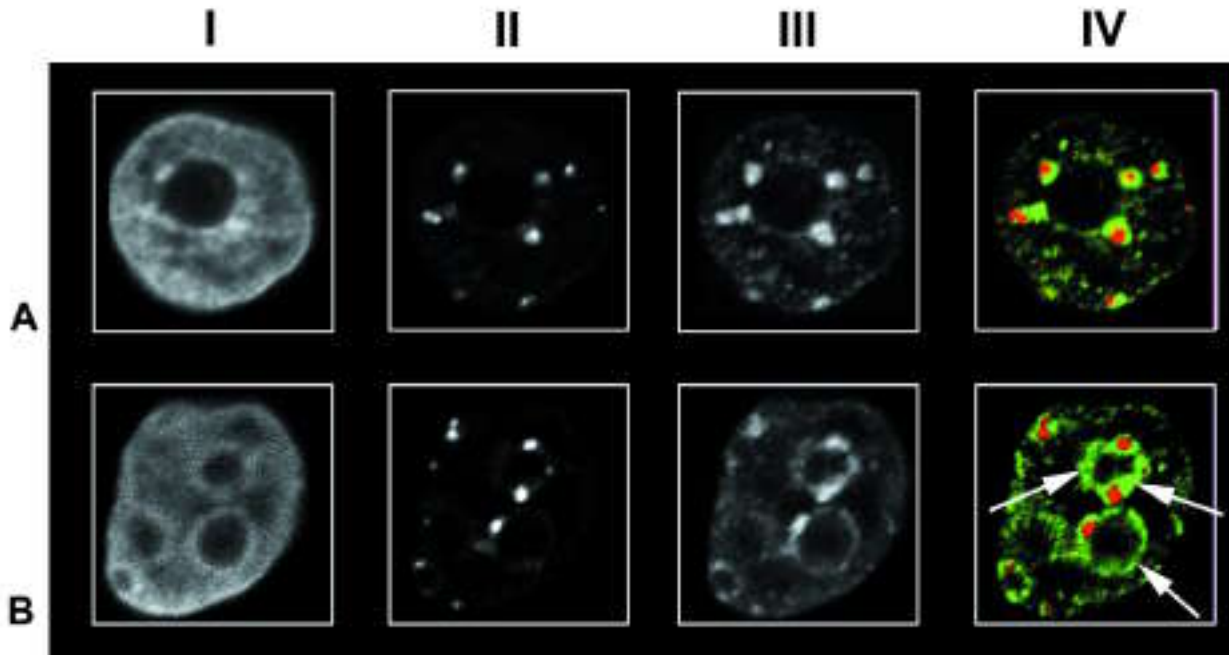
Figure 3. Simultaneous immunostaining of MML chromatin and centromeric regions in a confocal mid-section of a G0 nucleus (upper row) and an early S-phase nucleus (bottom row) of MCF-7 cells. Panel I: nuclear counterstain with TO-PRO-3, panel II: centromeres, panel III: heterochromatin visualized by metH3-K9, panel IV: merged image of MML chromatin in green, centromeres in red. Arrows indicate perinucleolar areas of MML chromatin not directly associated to centromeres.

mid-section of the nucleus after DNA counterstain, panel II shows the MML chromatin pattern of the corresponding section, panel III the pKi67 or BrdU patterns, respectively, and panel IV the merged image of MML chromatin with either pKi67 (panel IV A), BrdU (B and C) or with the nuclear counterstain (D). Visual inspection of nuclei from all cell cycle stages showed a fine granular or reticulated MML staining with low signal intensity expanding throughout the entire nucleus. The bulk MML chromatin with high signal intensity, however, revealed distinct differences during the cell cycle. In early $G_1$ (panel II A) numerous diffusely shaped MML chromatin clusters are scattered over the entire nucleus. An overlay of the pKi67 and MML chromatin patterns shows a high degree of colocalization of the pKi67 signals with these histone methylation sites (IV A). During early S-phase (panel B) the MML chromatin is preferentially located close to the nuclear periphery and around nucleoli. This space is largely devoid of early replicating chromatin as seen in the merged image by non-overlapping signals (IV B). Notably, the MML chromatin pattern seen in early S-phase is characteristic for chromatin replicating during mid S-phase (O'Keefe et al., 1992). This observation suggests that the MML chromatin

pattern in early S-phase *anticipates* the pattern of mid-replicating chromatin. The preferential localization around nucleoli and at the nuclear periphery is maintained during mid-S phase resulting in a partial colocalization or association of MML chromatin and mid-replicating chromatin (IV C). After exit of the cell cycle ($G_0$) MML labeled chromatin is concentrated in a few large, distinctly shaped compact clusters of high signal intensity in close association to the nucleoli and as a few smaller clusters at the nuclear periphery (IV D).

### *Topological relationship between MML chromatin patterns and centromeres*

In addition to the antibody against MML chromatin, MCF-7 cells were co- immunostained with a CREST antiserum that specifically binds to centromeric proteins such as CENP-A and CENP-B (Moroi et al., 1980) and thus delineates the kinteochores of centromeres (Figure 3). Panel I shows the nuclear DNA counterstain of a confocal mid-section, panel II the corresponding centromeric regions visualized by the CREST antiserum, panel III the MML chromatin pattern and panel IV the merged images of a $G_0$ nucleus (A) and an early S phase nucleus (B). Nuclei in $G_0$ were identified by the lack
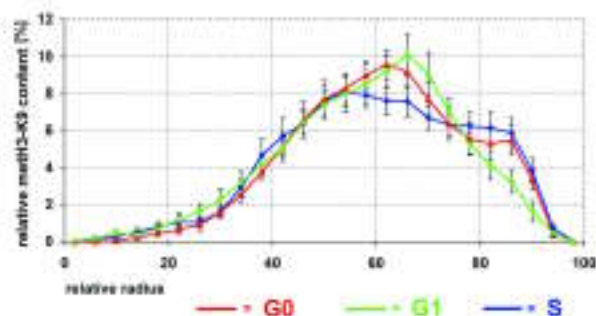
**Figure 4.** Quantitative 3D evaluation of radial distribution of MML labeled chromatin in 25 concentric shells after immunostaining in MCF-7 G0 nuclei (red), MCF-7 G1 nuclei (green) and MCF-7 S-phase nuclei (blue). The abscissa denotes the relative radius r of the nuclear shells, the ordinate the normalized sum of intensities in the voxels assigned to the color channel for MML chromatin. For normalization the area underlying each curve for the different series (total relative content of MML stained chromatin) was set to 100. Bars indicate standard deviations of the mean.

of immunostaining with pKi67 antibodies and nuclei in early S-phase by the typical pattern of incorporated BrdU (*not shown*). The nuclei revealed the typical MML chromatin patterns, described above for $G_0$ and early S-phase (compare Figure 2). In $G_0$ nuclei all clusters of centromeric kinetochores were closely associated to large MML chromatin clusters, which were located either around nucleoli or at the nuclear periphery. All MML labeled chromatin that was not associated with a centromere was seen as a fine granular pattern in the nucleus. In early S-phase, all centromeres were again found either at the nucleoli or at the nuclear periphery, within MML labeled chromatin compartments. However, a large fraction of intensely stained MML chromatin, not directly associated with centromeres was found in a ring shaped manner around the nucleoli and less distinctly at the nuclear periphery (Figure 3B, arrows). This suggests that the bulk of perinucleolar MML stained chromatin observed in early S-phase corresponds only to a minor fraction to the constitutive heterochromatin of centromeres.

### Approaches towards a quantitative 3D evaluation of the MML chromatin pattern

In an attempt to establish a quantitative 3D evaluation procedure to discriminate the different MML chromatin patterns observed during different cell cycle stages, the following parameters were analyzed in 3D images: (i) the radial distribution of MML chromatin clusters, e.g. their distribution as

a function of their distance from the nuclear center, (ii) the number of MML chromatin clusters (further referred to as objects) at different threshold levels, (iii) the density of MML chromatin objects expressed either by the mean ratio of the intensity per voxel from all voxels assigned to an object or by the mean ratio of the intensity per surface assigned to an object. These parameters are exemplified below for MCF-7 nuclei.

### i) Radial distribution of MML chromatin using fixed threshold levels

Prior to the evaluation of the radial distribution a threshold level of gray value was set manually for each individual nucleus with the objective to define chromatin that was unequivocally assigned to MML chromatin clusters. The threshold for different nuclei varied between 90 and 120. Figure 4 shows the curves for the radial distribution of MML labeled chromatin for the different cell cycle stages of the MCF-7 cell line. For each cell cycle stage 11 to 20 nuclei were evaluated. In each graph the normalized chromatin content, represented by its voxel-intensity weighted fluorochromes is plotted against the relative radius of the nucleus (*for details see methods*). These curves thus explore the positioning of MML chromatin with regard to the distance from the geometrical center of the nucleus. The MML chromatin pattern in $G_1$ nuclei closely resemble a Gaussian distribution, with its maximum at around 65% of the relative radius, whereas the pattern in $G_0$ nuclei shows two small peaks, the first around 62% and the second around 86% of the relative radius. With a maximum at around 52% of the relative radius, S-phase nuclei show the most internal position of MML chromatin, reflecting the accumulation around internally located nucleoli. Despite the remarkable differences of these patterns observed in different cell cycle stages by visual inspection, the two-sided Kolmogorov-Smirnov did not reveal significant differences.

### (ii) Number of MML chromatin objects defined at different threshold levels

In addition we assessed the number of MML stained objects. In such an analysis, one has to keep in mind that the threshold level for complex structures with a wide range of intensities is inevitably chosen arbitrarily and that different settings of the threshold level strongly influence the outcome of such an analysis. Figure 5 exemplifies this for one

nucleus. Figure 5 A shows a mid-section of the raw images of a $G_0$ MCF-7 nucleus after immunostaining with the MML antibody. As typically seen in this cell type, besides a number of sharply outlined large clusters with high signal intensity, a network of low intensity signals, sometimes forming ring like structures expands throughout the nucleus. These low intensity signals may reflect background, but they may also represent specific signals possibly reflecting small regions containing genes that are controlled by histone methylation. In panels 5 B-F the same nucleus is displayed with different threshold levels, marking voxels above the respective threshold in red (left-hand row). The resulting 3D objects after applying the object definition rules (see Materials and Methods) are shown in the right-hand row. Note that not every voxel above the threshold contributes to an object. While the number of marked voxels decreases constantly with increasing threshold levels, the number of objects initially increases at very low threshold levels until a maximum is reached (B-C). Thereafter the number of objects gradually starts to decrease with increasing threshold levels (C-E). Single objects, which consist of areas with heterogeneous intensities, can fall apart into several objects with increasing threshold levels, if they consist of voxels with heterogeneous intensities (compare objects marked with an arrow or an arrowhead in panels E and F of Figure 5). Figure 6 illustrates for three individual nuclei taken from cells at different cell cycle stages how the number of objects depends on the threshold value. The curve progression for the $G_0$ and the S-phase nucleus is much steeper compared to the $G_1$ nucleus. This indicates that these mainly large objects of $G_0$ and S-phase nuclei had a high degree of homogeneity, which decreased steadily in size over a wide range of thresholds and only at very high levels in number. In contrast, the more heterogeneous objects of $G_1$ nuclei tended to fall apart with higher thresholds compensating for a decrease of object numbers at these higher thresholds.

### (iii) Density of chromatin clusters visualized by MML immunostaining

In a further attempt to establish quantitative approaches that do not depend on one arbitrarily fixed threshold level, the average density of all segmented object voxels, either expressed by the intensity/voxel or by the intensity/surface (see methods part) was calculated over a wide range of threshold
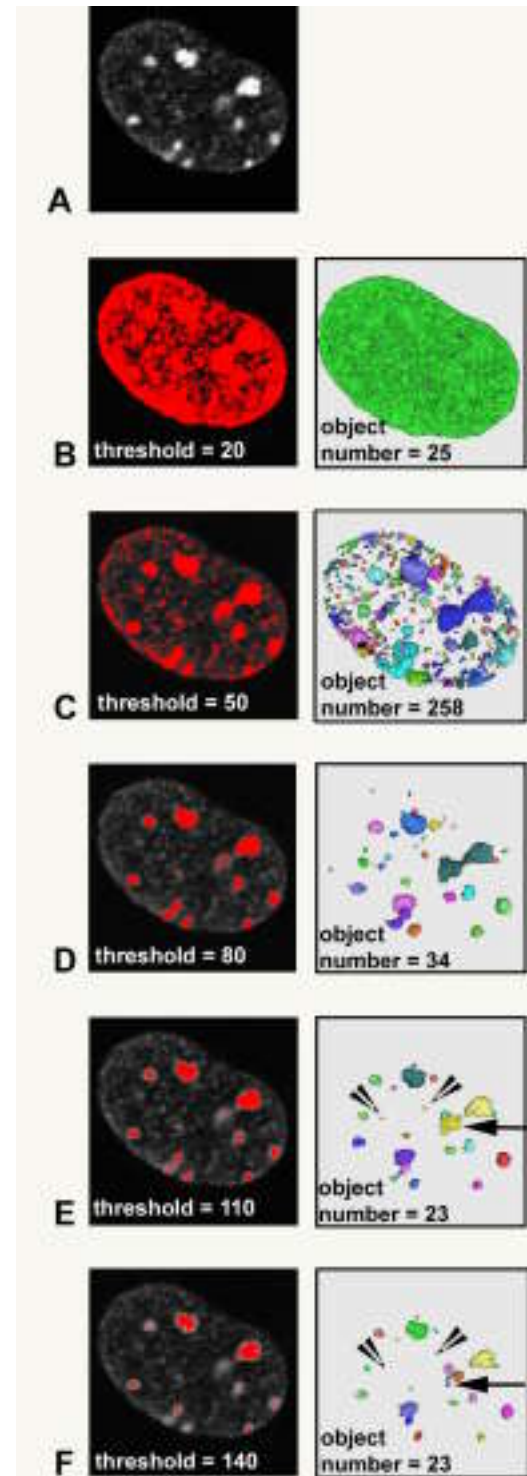


Figure 5. Segmentation of objects at different threshold levels. (A) mid-section of a raw image from confocal serial sections of a MCF-7 G0 nucleus. (B-F) the same nucleus is displayed with different threshold levels. Voxels above the respective threshold are marked in red on the left side images, the corresponding objects in varying colors on the right side images. Note that not all voxels above threshold contribute to an object due to the object definition as described in the methods part. For this particular nucleus an object maximum is obtained at a threshold around 50. The object number is the same at threshold levels 110 and 140 (E and F). This is due to a splitting of one larger object into several ones (marked by arrows) and the disappearance of objects between threshold levels 110 and 140 (marked by arrowheads).
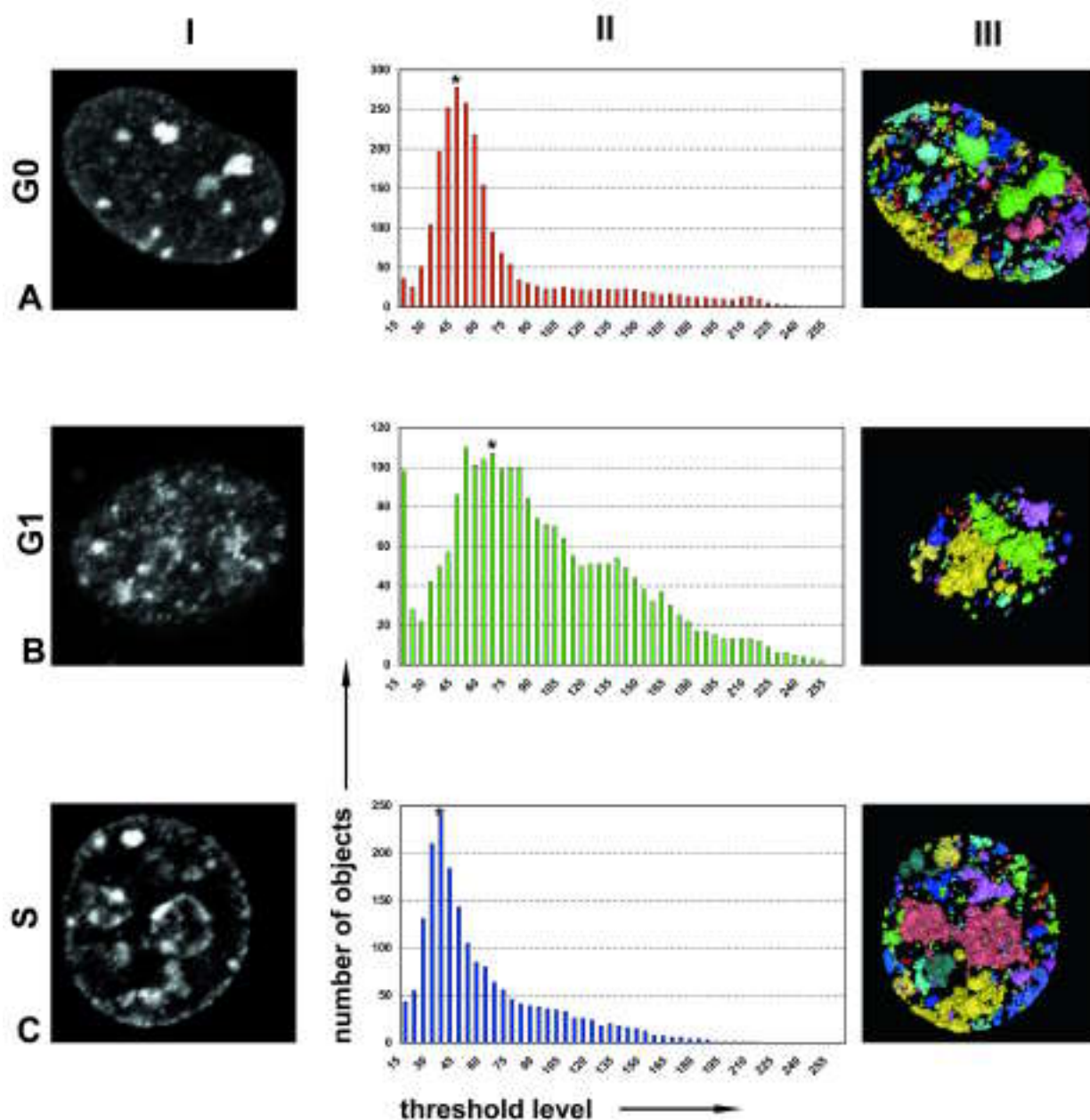
**Figure 6. Number of objects counted along threshold levels (gray values 15 to 255) of an MCF-7 G0 nucleus (A), an early G1 nucleus (B) and an early S-phase nucleus (C). Panel I shows a projection of 4 confocal mid-sections from each nucleus, encompassing 1μm of its central part, panel II the number of objects in each nucleus plotted against the threshold levels. In panel III the objects of the entire nucleus are displayed in 3D at threshold levels marked by an asterisk in the graphs.**

levels. This procedure was performed for each cell cycle stage of MCF-7 cells using the same set of nuclei described above for the evaluation of the radial distribution of MML chromatin (compare Figure 4). As shown in Figure 7 A the average intensity/voxel including all voxels assigned to an object was largely identical for all cell cycle stages over the entire range of threshold levels, demonstrating that the mean voxel intensity remains constant during the cell cycle. However, when the intensity/surface was plotted against threshold levels, (Figure 7 B), distinct differences between the cell cycle stages were found. The different values for $G_0$ nuclei compared to S and $G_1$ nuclei mirror the different degree of compactness in MML chromatin clusters during the respective cell cycle stages. The higher values for $G_0$ compared to S phase and $G_1$ nuclei indicate that objects in $G_0$ have the highest
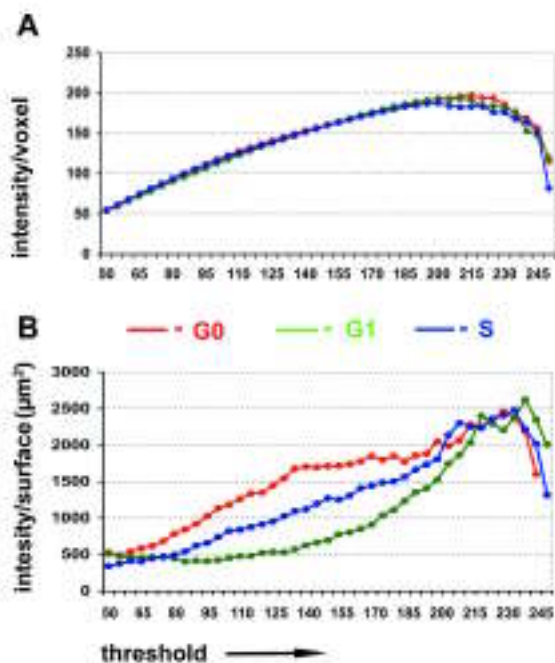
Figure 7. Evaluation of the density of objects. (A) the mean intensity/voxel averaged over all nuclei of a series is plotted against the threshold level. The ratio intensity/voxel increases with higher threshold levels since objects with a low intensity are eliminated. The decline of the curve at very high threshold levels is due to the fact that values are averaged over all nuclei within one series. At very high threshold levels some of the nuclei do not more display any objects, reducing the mean intensity/voxel. (B) The mean intensity/ surface averaged over all nuclei of a series is plotted against the threshold level.

and in $G_1$ the lowest compactness. Using the Mann-Whitney-U test the distribution curve for each cell cycle stage was significantly different ($p = 0.01$).

## Discussion

The observed MML chromatin pattern in $G_0$ nuclei of several normal and malignant cell types ranged from a fairly homogeneous distribution in normal lymphocytes to distinct cluster formation in monocytes, MCF-7 cells and Jurkat cells. In these cell types a dimorphic pattern of low intensity structures and of larger clusters with high signal intensity was observed. The latter were most prominent in the MCF-7 $G_0$ nuclei.

The transition from a homogeneous pattern in normal lymphocytes to the pronounced cluster formation observed in nuclei of the Jurkat cell line, which was established from a T-lymphocyte leukemia is striking. It remains speculative to what extent differences of MML chromatin patterns reflect the *chromosome level* or *gene level* function of histone

methylation (*see introduction*). High-intensity MML positive chromatin clusters, which are in addition to the di-methylation of H3-K9 probably also the result of a strong tri-methylation of H3-K27 and H4-K20 (Peters et al., 2003) may comprise both centromeric heterochromatin and surrounding facultative heterochromatin. The low intensity signals may represent a large number of smaller chromatin regions containing gene loci that are controlled by histone methylation of different lysines.

The distinct differences of MML chromatin patterns observed in $G_0$ nuclei from different cell types raise the question, whether these differences reflect cell type specific arrangements of chromosome territories (CTs). Present studies of CT arrangements in various normal and malignant cell types indicate highly variable neighborhoods of homologous and heterologous chromosomes (Bolzer et al., 2004; Cremer et al., 2001; Lesko et al., 1995; Sun and Yokota, 1999). In the light of these findings we consider it unlikely that cell type characteristic MML chromatin patterns can be explained as a consequence of cell type specific CT neighborhoods. In contrast to the high variability of CT neighborhoods, radial arrangements of CTs, defined as the distance from the nuclear center are highly nonrandom. These radial arrangements of CTs are size-correlated in fibroblast nuclei (Bolzer et al., 2004; Sun et al., 2000), but gene density correlated in nuclei such as lymphocytes and numerous others including MCF-7 cells (Boyle et al., 2001; Cremer et al., 2003; Kozubek et al., 2002) with a preferential location of gene poor CTs at the nuclear periphery and a preferential location of gene dense CTs in the nuclear interior. The quantitative evaluation of MML marked chromatin in MCF-7 cells, however, did not reveal a pronounced peripheral position. This was due to the major fraction of MML label found in large clusters around the nucleoli. These clusters contain also centromeric heterochromatin. Since centromeric regions are highly methylated at H3-K9 (Lachner and Jenuwein, 2002), an essential fraction of the MML chromatin pattern is reflected by the positions of centromeres. In $G_0$ lymphocytes the MML staining pattern was more intense in the nuclear periphery, which is in agreement with the peripheral location of centromeric heterochromatin in lymphocyte nuclei (Weierich et al., 2003). Possibly, major clusters of MML chromatin comprise higher order heterochromatin compartments built up from cen-

tromeric heterochromatin and facultative heterochromatic chromosomal subregions from neighboring CTs.

Little attention has been paid so far to changes of pattern formation of MML chromatin during and upon exit of the cell cycle. Our study demonstrates a profound change of the MML chromatin pattern in MCF-7 cells between early $G_1$ and S phase and after exit of the cell cycle. These changes were remarkable by visual inspection and confirmed by quantitative evaluation. This result raises several questions:

1. Do the observed cell cycle changes result from local changes in the level of methylation of H3-K9 and other methylated lysines in chromatin configurations that are stably positioned during interphase? Direct evidence for this assumption is lacking. Histone methylation is considered to be a very stable modification and potentially an irreversible epigenetic mark since histone demethylases have not been discovered so far. However, stably methylated histones might be removed by histone exchange eliminating their epigenetic potential (Sims et al., 2003).

2. Are cell cycle changes of MML patterns caused by large-scale changes of higher order chromatin arrangements during the cell cycle? Live cell observations of HeLa cells encompassing an entire cell cycle revealed, that — with the exception of the early $G_1$-phase (*see below*) — the position of chromosome territories and most chromosome subdomains are constrained within a range of about 1 µm from late $G_1$ until the end of $G_2$ (Walter et al., 2003). Further studies are indicated to test whether the large-scale stability of CT arrangements during the cell cycle is a general feature of mammalian cell nuclei. If this should be the case, the observed changes of the MML chromatin patterns during interphase in MCF-7 cells cannot be explained as a consequence of major changes of CT arrangements. Furthermore, studies of DNA-replication during S-phase provided evidence that replication foci do not undergo large-scale movements during S-phase. Instead replication factors are recruited to rather stably positioned chromatin foci (Leonhardt et al., 2000). However, while these observations argue against large scale movements of most chromatin from mid $G_1$ to late $G_2$, they do not exclude more expanded and possibly directed movements of a subset of defined subchromosomal regions. Centromeres provide a case in point. It has

recently been shown for a number of cell types, such as stimulated lymphocytes, lymphoblastoid cells, fibroblasts and a neuroblastoma cell line, that centromeres undergo major movements during the cell cycle and upon exit of the cell cycle ($G_0$ transition) (Solovei et al., 2004). In all cell types studied, centromeres were mostly found in the nuclear interior and partly at the nuclear periphery during early $G_1$, while in late $G_1$ most centromeres were seen as clusters at the periphery. This location was maintained through S-phase. Upon exit of the cell cycle ($G_0$ cells) centromeres were found in clusters at the nuclear periphery. A systematic quantitative analysis of centromere movements during the cell cycle in MCF-7 cells is still lacking. Since we found centromeric chromatin always in close association with MML labeled chromatin as demonstrated for a $G_0$ and an early S-phase nucleus, changes of MML chromatin patterns during the cell cycle may be explained in part by the dynamic behavior of centromeric chromatin.

3. The observed changes of MML chromatin patterns during the cell cycle lead to the question of a possible functional relevance. The remarkable association of MML chromatin sites and pKi67 during early $G_1$ may reflect the necessity of chromosome territories to home in to their final nuclear location and to establish a polarized orientation of CTs to expose chromosomal subregions with different transcriptional activity in a spatially correct manner (Sadoni et al., 1999; Walter et al., 2003). It has been shown that pKi67 interacts with HP-1, a protein that is recruited at metH3-K9 heterochromatin sites. A transient colocalization of HP-1 and pKi67 in heterochromatin foci was observed during telophase and early $G_1$ (Kametaka et al., 2002; Scholzen et al., 2002) suggesting a possible docking mechanism for heterochromatin in the newly developing nucleus. On the other side HP-1 interacts with the lamin B receptor, an integral component of the inner nuclear membrane (for review see Lachner and Jenuwein, 2002). During mitosis, HP-1 largely dissociates from chromosomes and reassembles at the polar surfaces of anaphase chromosomes (Kourmouli et al., 2000), whereas p-Ki-67 remains closely associated around chromosomes during this period. It is tempting to speculate that the pKi67/HP-1/metH3-K9 complex plays a role in reestablishing heterochromatin domains during telophase/early $G_1$ in a coordinated way with the HP-1 mediated binding of metH3-K9 marked hete-

rochromatin to the newly formed lamin B at the nuclear envelope (Schermelleh, 2003).

The present data emphasize the importance of further studies of nuclear architecture changes correlated with specific epigenetic chromatin modifications such as histone methylations at defined lysine positions. So far studies are still based to a large part on the qualitative assessment of the staining patterns observed in light optical nuclear sections. To overcome the subjectivity involved in such studies, the development of bioimaging approaches, which guarantee an impartial quantitative analysis of chromatin pattern formation with specific epigenetic marks in space and time is a demanding but requisite task. From the technical point of view a major obstacle for quantitative evaluations of fluorescently labeled objects in a nucleus is the need of setting a threshold in order to discriminate specific, segmented signals from unspecific background. This problem becomes crucial when numerous targets with complex structures and a wide range of signal intensities have to be segmented in the same nucleus. Both, automatic and interactive approaches for segmentation have their drawbacks (for review see Gil et al., 2002). A high threshold level may assure that no unspecific background signal is included in the evaluation. On the other hand, low intensity signals, which would be eliminated by a high threshold setting, may in fact be specific signals, which should not be ignored since they may have important functional implications. The importance of utilizing the full range of intensities has been shown by Fay et al. (1997) for an accurate quantitative analysis of the nuclear distribution of nascent RNA and the splicing factor SC-35. Approaches that are not limited to a fixed threshold and allow analyses along all levels of threshold settings should therefore preferably be implemented.

## References

Bird A. DNA methylation patterns and epigenetic memory. Genes Dev 2002;16:6-21.

Bolzer A, Kreth G, Solovei I, Saracoglu K, Fauth C, Müller S, et al. Complete 3D maps of chromosome positions in human male fibroblast nuclei and prometaphase rosettes demonstrate a size dependent, probabilistic arrangement. Submitted 2004.

Boyle S, Gilchrist S, Bridger JM, Mahy NL, Ellis JA, Bickmore WA. The spatial organization of human chromosomes within the nuclei of normal and emerin-mutant cells. Hum Mol Genet 2001;10:211-9.

Cremer M, Kupper K, Wagler B, Wizelman L, Hase Jv J, Weiland Y, et al. Inheritance of gene density-related higher order chromatin arrangements in normal and tumor cell nuclei. J Cell Biol 2003;162:809-20.

Cremer M, von Hase J, Volm T, Brero A, Kreth G, Walter J, et al. Non-random radial higher-order chromatin arrangements in nuclei of diploid human cells. Chromosome Res 2001;9:541-67.

Diaz G, Zucca A, Setzu MD, Cappai C. Chromatin pattern by variogram analysis. Microsc Res Tech 1997;39:305-11.

Elgin SC, Grewal SI. Heterochromatin: silence is golden. Curr Biol 2003;13:R895-8.

Fay FS, Taneja KL, Shenoy S, Lifshitz L, Singer RH. Quantitative digital analysis of diffuse and concentrated nuclear distributions of nascent transcripts, SC35 and poly(A). Exp Cell Res 1997;231:27-37.

Gerdes J, Lemke H, Baisch H, Wacker HH, Schwab U, Stein H. Cell cycle analysis of a cell proliferation-associated human nuclear antigen defined by the monoclonal antibody Ki-67. J Immunol 1984;133:1710-5.

Gil J, Wu H, Wang BY. Image analysis and morphometry in the diagnosis of breast cancer. Microsc Res Tech 2002;59:109-18.

Heitz E. Das Heterochromatin der Moose. I. Jahrb. Wiss Botanik 1928;69:762-818.

Jones PA, Baylin SB. The fundamental role of epigenetic events in cancer. Nat Rev Genet 2002;3:415-28.

Kametaka A, Takagi M, Hayakawa T, Haraguchi T, Hiraoka Y, Yoneda Y. Interaction of the chromatin compaction-inducing domain (LR domain) of Ki-67 antigen with HP1 proteins. Genes Cells 2002;7:1231-42.

Kourmouli N, Theodoropoulos PA, Dialynas G, Bakou A, Politou AS, Cowell IG, et al. Dynamic associations of heterochromatin protein 1 with the nuclear envelope. Embo J 2000;19:6558-68.

Kozubek S, Lukasova E, Jirsova P, Koutna II, Kozubek M, Ganova A, et al. 3D Structure of the human genome: order in randomness. Chromosoma 2002;111:321-31.

Lachner M, Jenuwein T. The many faces of histone lysine methylation. Curr Opin Cell Biol 2002;14:286-98.

Lachner M, O'Carroll D, Rea S, Mechtler K, Jenuwein T. Methylation of histone H3 lysine 9 creates a binding site for HP1 proteins. Nature 2001;410:116-20.

Lachner M, O'Sullivan RJ, Jenuwein T. An epigenetic road map for histone lysine methylation. J Cell Sci 2003;116:2117-24.

Leonhardt H, Rahn HP, Weinzierl P, Sporbert A, Cremer T, Zink D, et al. Dynamics of DNA replication factories in living cells. J Cell Biol 2000;149:271-80.

Lesko SA, Callahan DE, LaVilla ME, Wang ZP, Ts'o PO. The experimental homologous and heterologous separation distance histograms for the centromeres of chromosomes 7, 11, and 17 in interphase human T-lymphocytes. Exp Cell Res 1995;219:499-506.

Mairinger T, Mikuz G, Gschwendtner A. Nuclear chromatin texture analysis of nonmalignant tissue can detect adjacent prostatic ade-

nocarcinoma. Prostate 1999;41:12-9.

Moroi Y, Peebles C, Fritzler MJ, Steigerwald J, Tan EM. Autoantibody to centromere (kinetochore) in scleroderma sera. Proc Natl Acad Sci USA 1980;77:1627-31.

Mulder JW, Offerhaus GJ, de Feyter EP, Floyd JJ, Kern SE, Vogelstein B, et al. The relationship of quantitative nuclear morphology to molecular genetic alterations in the adenoma-carcinoma sequence of the large bowel. Am J Pathol 1992;141:797-804.

Muller S, Eder V, Wienberg J. A nonredundant multicolor bar code as a screening tool for rearrangements in neoplasia. Genes Chromosomes Cancer 2004;39:59-70.

O'Keefe RT, Henderson SC, Spector DL. Dynamic organization of DNA replication in mammalian cell nuclei: spatially and temporally defined replication of chromosome-specific α-satellite DNA sequences. J. Cell Biol 1992;116:1095-110.

Perez-Burgos L, Peters A, Opravil S, Kauer M, Mechtler K, Jenuwein T. Generation and characterization of methyl-lysine antibodies. Methods Enzymol 2004; 376:234-54.

Peters AH, Kubicek S, Mechtler K, O'Sullivan RJ, Derijck AA, Perez-Burgos L, et al. Partitioning and plasticity of repressive histone methylation states in mammalian chromatin. Mol Cell 2003;12:1577-89.

Plath K, Fang J, Mlynarczyk-Evans SK, Cao R, Worringer KA, Wang H, et al. Role of histone H3 lysine 27 methylation in X inactivation. Science 2003;300:131-5.

Sadoni N, Langer S, Fauth C, Bernardi G, Cremer T, Turner BM, et al. Nuclear organization of mammalian genomes. Polar chromosome territories build up functionally distinct higher order compartments. J Cell Biol 1999;146:1211-26.

Schermelleh L. Dynamic organization of chromosomes in the mammalian cell nucleus. (Dissertation, Univ. of Munich 2003).

Schneider U, Schwenk HU, Bornkamm G. Characterization of EBV-genome negative "null" and "T" cell lines derived from children with acute lymphoblastic leukemia and leukemic transformed non-Hodgkin's lymphoma. Int J Cancer 1977;19:621-6.

Scholzen T, Endl E, Wohlenberg C, van der Sar S, Cowell IG, Gerdes J, et al. The Ki-67 protein interacts with members of the heterochromatin protein 1 (HP1) family: a potential role in the regulation of higher-order chromatin structure. J Pathol 2002;196:135-44.

Sims RJ 3rd, Nishioka K, Reinberg D. Histone lysine methylation: a signature for chromatin function. Trends Genet 2003;19:629-39.

Solovei I, Schermelleh L, Düring K, Engelhardt A, Stein S, Von Hase J, et al. Differences in centromere position during cell cycle and at Go in four different types of human cells. (submitted 2004).

Sun HB, Shen J, Yokota H. Size-dependent positioning of human chromosomes in interphase nuclei. Biophys J 2000;79:184-90.

Sun HB, Yokota H. Correlated positioning of homologous chromosomes in daughter fibroblast cells. Chromosome Res 1999;7:603-10.

Tashiro S, Walter J, Shinohara A, Kamada N, Cremer T. Rad51 accumulation at sites of DNA damage and in postreplicative chromatin. J Cell Biol 2000;150:283-91.

Walter J, Schermelleh L, Cremer M, Tashiro S, Cremer T. Chromosome order in HeLa cells changes during mitosis and early G1, but is stably maintained during subsequent interphase stages. J Cell Biol 2003;160:685-97.

Weierich C, Brero A, Stein S, von Hase J, Cremer C, Cremer T, et al. Three-dimensional arrangements of centromeres and telomeres in nuclei of human and murine lymphocytes. Chromosome Res 2003; 11:485-502.

Weyn B, Jacob W, da Silva VD, Montironi R, Hamilton PW, Thompson D, et al. Data representation and reduction for chromatin texture in nuclei from premalignant prostatic, esophageal, and colonic lesions. Cytometry 2000;41:133-8.